

**DOT/FAA/AR-03/57**

Office of Aviation Research  
Washington, D.C. 20591

# **Failure Modeling of Titanium 6Al-4V and Aluminum 2024-T3 With the Johnson-Cook Material Model**

September 2003

Final Report

This document is available to the U.S. public  
through the National Technical Information  
Service (NTIS), Springfield, Virginia 22161.



U.S. Department of Transportation  
**Federal Aviation Administration**

## **NOTICE**

This document is disseminated under the sponsorship of the U.S. Department of Transportation in the interest of information exchange. The United States Government assumes no liability for the contents or use thereof. The United States Government does not endorse products or manufacturers. Trade or manufacturer's names appear herein solely because they are considered essential to the objective of this report. This document does not constitute FAA certification policy. Consult your local FAA aircraft certification office as to its use.

This report is available at the Federal Aviation Administration William J. Hughes Technical Center's Full-Text Technical Reports page: [actlibrary.tc.faa.gov](http://actlibrary.tc.faa.gov) in Adobe Acrobat portable document format (PDF).

1. Report No. DOT/FAA/AR-03/57	2. Government Accession No.	3. Recipient's Catalog No.	
4. Title and Subtitle FAILURE MODELING OF TITANIUM 6Al-4V AND ALUMINUM 2024-T3 WITH THE JOHNSON-COOK MATERIAL MODEL		5. Report Date September 2003	6. Performing Organization Code
		8. Performing Organization Report No.	
7. Author(s) Gregory Kay	9. Performing Organization Name and Address Lawrence Livermore National Laboratory P.O. Box 808 Livermore, CA 94551		
12. Sponsoring Agency Name and Address U.S. Department of Transportation Federal Aviation Administration Office of Aviation Research Washington, DC 20591		10. Work Unit No. (TRAIS)	11. Contract or Grant No.
		13. Type of Report and Period Covered Final Report	
15. Supplementary Notes The FAA William J. Hughes Technical Center COTR was Don Altobelli.		14. Sponsoring Agency Code ANE-100, ANM-100	
		16. Abstract Johnson-Cook failure strain parameters were developed for Ti-6Al-4V and 2024-T3 aluminum. The titanium parameters, obtained from simulations of split Hopkinson bar tensile tests, were successfully used to simulate blade fragment impact tests on 0.602", 0.250", and 0.737" thick titanium targets. Titanium failure parameters that were derived from scaled down ballistic limit testing produced a failure envelope which was not suitable for use on full-scale tests. 2024-T3 aluminum failure parameters were obtained from simulations of one-third-scale ballistic limit test results. The aluminum failure parameters were used to simulate three blade fragment impact tests against a commercial transport aircraft fuselage.	
17. Key Words Johnson-Cook failure strain parameters, Titanium 6Al-4V, 2024-T3 aluminum		18. Distribution Statement This document is available to the public through the National Technical Information Service (NTIS) Springfield, Virginia 22161.	
19. Security Classif. (of this report) Unclassified	20. Security Classif. (of this page) Unclassified	21. No. of Pages 24	22. Price

## ACKNOWLEDGMENTS

This work was performed under the auspices of the U.S. Department of Energy by the Lawrence Livermore National Laboratory (LLNL) under contract No. W-7405-ENG-48. The author is indebted to Donald Lesuer and Mary LeBlanc for the split Hopkinson bar testing and to Ray Gogolewski and Bruce Morgan for the ballistic limit testing, all of which was performed at LLNL. Thanks also go to Steve Lundin at the Naval Air Warfare Center China Lake for the fan blade/fuselage testing data and to D.G. Alexander and L.M. Dietz from Pratt & Whitney for the blade/containment target data. Rich Couch was the program manager for the FAA-sponsored project at LLNL.

## TABLE OF CONTENTS

	Page
EXECUTIVE SUMMARY	vii
1. INTRODUCTION	1
1.1 Purpose	1
1.2 Johnson-Cook Material Model	1
1.3 Johnson-Cook Failure Model	2
2. FAILURE STRAIN PARAMETERS FOR Ti6Al-4V	3
2.1 Ti-6Al-4V Failure Parameter Determination	3
2.2 Scaled Down Ballistic Limit Tests	3
2.3 Split Hopkinson Bar Tests	4
2.4 Ti-6Al-4V Failure Parameter Evaluation	8
2.5 Convergence Issues	11
3. 2024-T3 ALUMINUM FAILURE STRAIN PARAMETERS	12
3.1 2024-T3 Auminum Failure Parameter Determination	12
3.2 2024-T3 Aluminum Failure Parameter Evaluation	14
4. SUMMARY	16
5. REFERENCES	17

## LIST OF FIGURES

Figures	Page
1 Stress-Strain Results for the 0.025" Notch Radius Ti-6Al-4V Tensile Hopkinson Bar Test	5
2 Stress-Strain Results for the 0.050" Notch Radius Ti-6Al-4V Tensile Hopkinson Bar Test	6
3 Johnson-Cook Ti-6Al-4V Flow Surfaces for Varying Strain Rates	6
4 Johnson-Cook Ti-6Al-4V Failure Strains for Varying $\sigma^*$	7

5	Calculated Stress Comparisons for the 0.025" Notch Radius Ti-6Al-4V Tensile Hopkinson Bar Test	7
6	Calculated Stress Comparisons for the 0.050" Notch Radius Ti-6Al-4V Tensile Hopkinson Bar Test	8
7	Crack Pattern Produced by the Johnson-Cook Model and the Observed Pattern for P&W Titanium Blade Impact Test 5	9
8	Crack Pattern Produced by the Johnson-Cook Model and the Observed Pattern for P&W Titanium Blade Impact Test 3	10
9	Naval Air Warfare Center China Lake Titanium Panel Impact Test 16	11
10	2024-T3 Ballistic Limit Simulation Comparisons With LLNL Experimental Results	12
11	Johnson-Cook 2024-T3 Flow Surfaces for Varying Strain Rates	13
12	Johnson-Cook 2024-T3 Aluminum Failure Strains for Varying $\sigma^*$	13
13	Naval Air Warfare Center Engine Debris Test 17: Fan Blade Fragment Impact With a Skin Section	15
14	Naval Air Warfare Center Engine Debris Test 22: Fan Blade Impact With a Skin/Hat Section	15
15	Naval Air Warfare Center Engine Debris Test 14: Fan Blade Impact With a Skin/Rib Section	16

## LIST OF TABLES

Tables	Page	
1	Solution Convergence Issues Were Simplified After Maintaining Close to Uniform Mesh Resolution for the Ti-6Al-4V Simulations	11
2	Solution Convergence Issues Were Simplified After Maintaining Close to Uniform Mesh Resolution for the 2024-T3 Aluminum Simulations	14

## EXECUTIVE SUMMARY

A validated Johnson-Cook model could be employed to perform simulations relating to the containment aspects of aircraft and engine designs. This report describes the determination and evaluation of the parameters that can be used to predict failure in Ti-6Al-4V and 2024-T3 aluminum. The titanium parameters in this study were obtained from manually optimized simulations of split Hopkinson bar tensile tests. The aluminum failure parameters were obtained from optimized simulations of one-third-scale ballistic limit test results. The failure parameters for both materials were validated on full-scale penetration tests.

Ti-6Al-4V failure parameters that were derived from scaled down ballistic limit testing produced a failure envelope that was not suitable for use on full-scale tests. The Ti-6Al-4V parameters derived from scaled down tests were also not consistent with those determined by Hopkinson bar tests. Failure mode identification, material processing, and rate effects are possible causes for this inconsistency and it is recommended that further investigation be initiated to assure validation for the ongoing Federal Aviation Administration William J. Hughes Technical Center Aircraft Catastrophic Failure Prevention Program.

## 1. INTRODUCTION.

### 1.1 PURPOSE.

A validated Johnson-Cook model could be employed to perform simulations that conform to Federal Aviation Administration standards for evaluating aircraft and engine designs for airworthiness and containment considerations. A previous Lawrence Livermore National Laboratory (LLNL) report [1] described the motivation for using the Johnson-Cook material model in simulations involving engine containment and the effect of uncontained engine debris on aircraft structures. In that report, experimental studies of the deformation and failure behavior of Ti-6Al-4V and 2024-T3 aluminum at high strain rates and large strains were conducted. That report also describes the generation of material constants for the Johnson-Cook strength model. This report describes the determination and evaluation of the parameters for Ti-6Al-4V and 2024-T3 aluminum that can be used in the failure portion of the Johnson-Cook material.

### 1.2 JOHNSON-COOK MATERIAL MODEL.

The Johnson-Cook Flow Surface is:

$$\sigma_{yield} = [A + B(\bar{\epsilon}^p)^n][1 + C \ln(\dot{\epsilon}^*)][1 + (T^*)^m]$$

where  $A$ ,  $B$ ,  $C$ ,  $n$  and  $m$  are constants.

The nondimensional temperature

$$T^* = \frac{T - T_{room}}{T_{melt} - T_{room}}$$

where  $T$  is the current temperature,  $T_{room}$  is the ambient temperature, and  $T_{melt}$  is the melt temperature. Adiabatic conditions are assumed such that all internal plastic work is converted into temperature change, i.e.

$$\Delta T = \frac{\bar{\sigma} \bar{\epsilon}^p}{\rho C_v}$$

where  $\bar{\sigma}$  is the effective stress,  $\bar{\epsilon}^p$  is the effective plastic strain,  $\rho$  is the mass density, and  $C_v$  is the constant volume specific heat. The effective plastic strain  $\bar{\epsilon}^p$  is defined by

$$\bar{\epsilon}^p = \int_0^t d\bar{\epsilon}^p$$

where the incremental plastic strain  $d\bar{\epsilon}^p$  is determined from the incremental plastic strain tensor  $d\epsilon_{ij}$ , such that

$$d\bar{\epsilon}^p = \sqrt{\frac{2}{3}} d\epsilon_{ij} d\epsilon_{ij}$$

The effective stress  $\bar{\sigma}$  is defined by

$$\bar{\sigma} = \sqrt{\frac{3}{2}} \sigma_{ij} \sigma_{ij}$$

The nondimensional strain rate  $\dot{\epsilon}^*$  is the ratio of the effective plastic strain rate  $\dot{\bar{\epsilon}}^p$  to the reference strain rate  $\dot{\epsilon}^0$  (usually equal to 1.0), i.e.

$$\dot{\epsilon}^* = \frac{\dot{\bar{\epsilon}}^p}{\dot{\epsilon}^0}$$

### 1.3 JOHNSON-COOK FAILURE MODEL.

Failure accumulation in the Johnson-Cook model does not directly degrade the yield surface. The model, more fully described in reference 2, defines the strain at fracture as

$$\epsilon_{failure} = [D_1 + D_2 \exp(D_3 \sigma^*)] [1 + D_4 \ln(\dot{\epsilon}^*)] [1 + D_5 T^*]$$

where  $\sigma^*$  is the ratio of the pressure to the effective stress, i.e.

$$\sigma^* = \frac{pressure}{\bar{\sigma}}$$

Fracture occurs in the Johnson-Cook model when the damage parameter  $D$  exceeds 1.0. The evolution of  $D$  is given by the accumulated incremental effective plastic strains divided by the current strain at fracture

$$D = \sum \frac{\Delta \bar{\epsilon}^p}{\epsilon_{failure}}$$

During the calculation, element stresses are all set to zero and remain equal to zero when the fracture criteria is evoked for a specific element.

The first set of brackets in the Johnson-Cook fracture model are intended to represent the observation that the strain to fracture decreases as the hydrostatic tension increases [3]. The second set of brackets in the strain to failure expression represent the effect of an increased strain rate on the material ductility, while the third set of brackets represent the effect of thermal softening on the material ductility. Johnson-Cook failure parameters for the two materials in this study have previously been published [4], but they were determined in conjunction with strength model parameters, which are different from those employed in this study [1].

Failure strain dependency on the state of hydrostatic tension was considered in this study, i.e.

$$\varepsilon_{failure} = [D_1 + D_2 \exp(D_3 \sigma^*)] D^*$$

where  $D^*$  is a constant. Failure strain parameters that are concerned with the strain rate and temperature,  $D_4$  and  $D_5$ , were drawn from reference 4. The consequence of this restriction, imposed by the scope of the study, was diminished by the observation that the tests used to determine  $D_1$ ,  $D_2$ , and  $D_3$  were conducted at strain rates approximately equal to those encountered in the full-scale tests. The  $D_1$ ,  $D_2$ , and  $D_3$  failure parameters were determined for each material by careful parameter adjustment until a manually optimized correlation was obtained with the appropriate split Hopkinson bar and ballistic limit tests. Several attempts were made to employ an optimizer code to accomplish the parameter determination, but they ultimately did not prove as useful as the manual optimization. The primary difficulty that was encountered in the optimizer code application was the definition of a viable metric (for both the ballistic limit and the Hopkinson bar simulations) that was sensitive to reasonable parameter space variations.

## 2. FAILURE STRAIN PARAMETERS FOR Ti6Al-4V.

### 2.1 Ti-6Al-4V FAILURE PARAMETER DETERMINATION.

The Ti-6Al-4V failure strain parameters for the Johnson-Cook failure model were determined by simulating the results of tensile Hopkinson bar tests employing 0.312" diameter specimen geometries and notch radii of either 0.025" or 0.050". The different notch radii provided a multiaxial loading range, as defined by  $\sigma^*$ , similar to that expected in the full-scale penetration verification tests. The calculated stress and strain across the notch was compared to the measured stress and strain for a complete set of failure strain parameters ( $D_1$ - $D_3$ ). These failure strain parameter sets were then varied until a satisfactory fit to the data was obtained. The parameters that were obtained from the Hopkinson bar tests were evaluated on two Pratt & Whitney (P&W) blade fragment tests with 0.601" and 0.737" thick targets and a Naval Air Warfare Center (NAWC) China Lake-supplied blade fragment tested on a 0.250" thick titanium target.

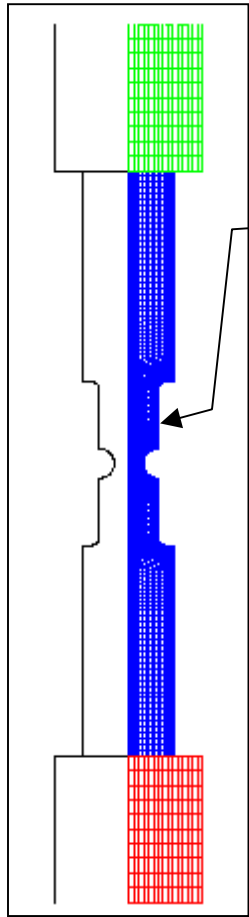
### 2.2 SCALED DOWN BALLISTIC LIMIT TESTS.

Initially, Ti-6Al-4V failure parameters were derived from ballistic limit test data of fixed 6" by 6" by 0.250" thick targets that were impacted by 0.58" diameter by 8.7" long right-circular cylinders [5]. These initial failure parameters produced a failure envelope that was not suitable for the simulation of the full-scale penetration tests that were performed by P&W [6] and the NAWC China Lake [7], i.e., the parameters predicted material responses that were much tougher than reality. This inconsistency could be attributed to the prediction of plugging or shear localization target failure with parameters that are based primarily on a material undergoing petaling (tearing) failure. The targets under consideration in this report can be classified [8] as being intermediate (the rear surface exerts influence on the penetration process) to thick (influence of the boundary is felt only after substantial target penetration). For these targets, a

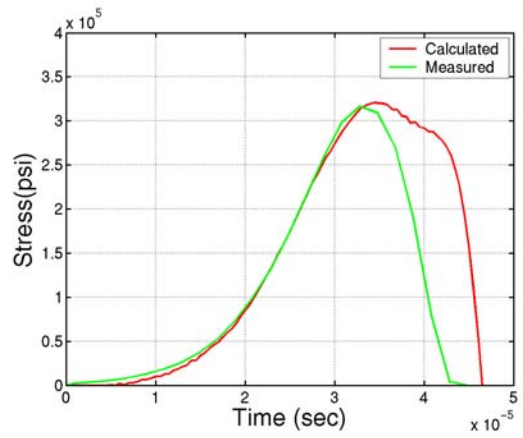
pronounced change in slope had been reported [9] when the ballistic limit velocity is plotted against the target areal weight (mass density times thickness). This change in slope, attributed to a change in target failure mode from petaling to plugging, tends to flatten out the response curve, producing a decreasing change in ballistic limit with increasing target areal density. Thus, "...it appears that a smaller percentage of the projectile's kinetic energy at impact is transferred to the plate when the plate undergoes a shear (plug) mode failure than when it undergoes a petal (tear) mode failure. This implies that projectile limit speed could be lower for a shear failure than for a petal failure all else held constant (i.e., if the plate had a choice of failure mode)" [5]. The inconsistency from using scaled down ballistic limit data on full-size events could also be due to material processing or loading rates. This situation merits further investigation into the condition of the material and the ability of the model to distinguish between failure modes. The initial Ti-6Al-4V failure parameters were also not consistent with the parameters determined later by the tensile Hopkinson bar tests.

### 2.3 SPLIT HOPKINSON BAR TESTS.

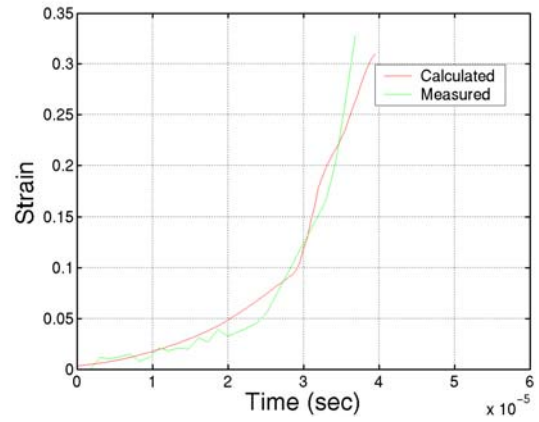
Stress and strain data were collected at two specimen locations in the Hopkinson bar tensile tests. Specimen stress-time histories were inferred from strain gauge data that was recorded on a transmitter bar that was attached to the tensile specimen. Strain-time histories were inferred from optical results of a framing camera looking at notch elongations during the passage of the tensile waves. These two signals were cross plotted, after adjusting for the time delays due to the separation of the data recording locations. This somewhat subjective procedure was duplicated in the simulations, where elongation was measured and compared to the original notch gauge length for strain, and the strain at the transmitter bar was converted to stress to infer uniaxial stress conditions in the specimen. The two-dimensional mesh that was employed in these simulations is shown in figure 1, as are the stress and strain comparisons with the data for the small radius specimens. The stress and strain comparisons for the large notch case are shown in figure 2. The small radius specimen had a notch radius of 0.25" and a nominal diameter of 0.100", and the large radius specimen had a notch radius of 0.500" and a nominal diameter of 0.100". Failure parameters were developed that bounded the results for both notch cases, i.e., +5.9% error for the small notch and -5.8% error for the large notch. The failure parameters that were obtained by the Hopkinson bar test simulations are given in figure 4. The flow surface, from reference 1, that was used in the simulations is shown in figure 3.



Measured extensional strain across the notch was 0.320", the calculated strain was 0.339", a 5.9% error

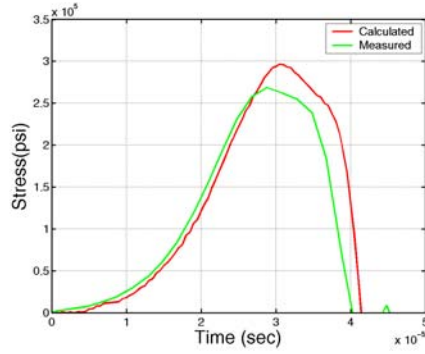


Stress-time history of the transmitter bar strain gauge

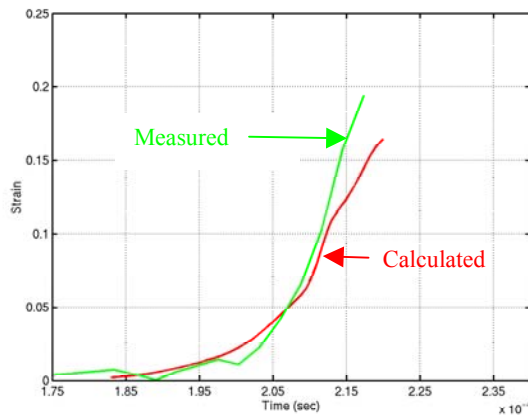


Strain-time history across the notch

FIGURE 1. STRESS-STRAIN RESULTS FOR THE 0.025" NOTCH RADIUS Ti-6Al-4V TENSILE HOPKINSON BAR TEST



Stress-time history of the transmitter bar strain gauge



Strain-time history across the notch

FIGURE 2. STRESS-STRAIN RESULTS FOR THE 0.050" NOTCH RADIUS Ti-6Al-4V TENSILE HOPKINSON BAR TEST

Titanium 6Al-4V yield surface parameters [1]

$A = 159.246 \text{ ksi}$     $n = 0.93$

$B = 158.376 \text{ ksi}$     $m = 1.1$

$C = 0.014$

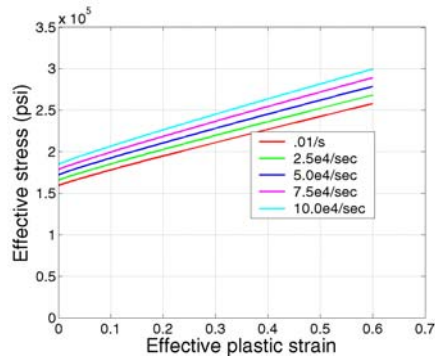


FIGURE 3. JOHNSON-COOK Ti-6Al-4V FLOW SURFACES FOR VARYING STRAIN RATES

Titanium 6Al-4V failure strain parameters

$$D_1 = -0.090 \quad D_4 = 0.014$$

$$D_2 = 0.270 \quad D_5 = 3.870$$

$$D_3 = 0.480$$

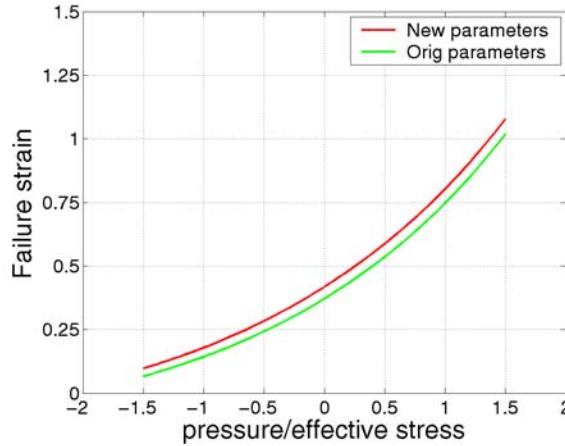


FIGURE 4. JOHNSON-COOK Ti-6Al-4V FAILURE STRAINS FOR VARYING  $\sigma^*$

The assumption of a dynamic homogeneous response may be reasonable for small uniform specimens (prior to necking) in split Hopkinson bar tests, but the existence of a notch certainly raises issues about a similar assumption for the above tests. The change in effective stress across the notches in the above tests can be seen in figures 5 and 6, as well as the average stresses calculated for the transmitter bar. As can be seen, the calculated effective stresses across the notches are fairly uniform, but they do differ from the transmitter bar stresses (which are used in the experimental results). This difference was considered intrinsic to the use of a Hopkinson bar test using notched specimens. Local and average strain rates also differ, the maximum extensional strain rates as measured during the tests were  $6800 \text{ sec}^{-1}$  and  $4300 \text{ sec}^{-1}$  for the small and large radii specimens respectively, while the maximum calculated local strains rates for the same specimens were  $13,500 \text{ sec}^{-1}$  and  $10,700 \text{ sec}^{-1}$ .

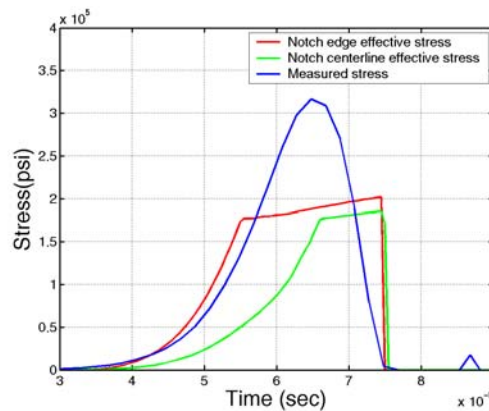


FIGURE 5. CALCULATED STRESS COMPARISONS FOR THE 0.025" NOTCH RADIUS Ti-6Al-4V TENSILE HOPKINSON BAR TEST

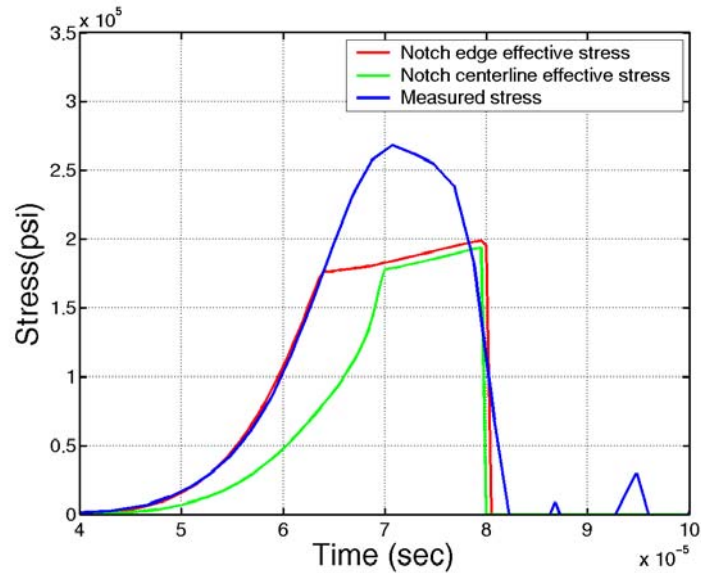


FIGURE 6. CALCULATED STRESS COMPARISONS FOR THE 0.050" NOTCH RADIUS Ti-6Al-4V TENSILE HOPKINSON BAR TEST

#### 2.4 Ti-6Al-4V FAILURE PARAMETER EVALUATION.

The failure strain parameters obtained from the tensile Hopkinson bar tests were evaluated on penetration tests performed by P&W [6] and the NAWC China Lake [7]. The P&W test targets were rolled plate Ti-6Al-4V with a specification of AMS 4911 in thicknesses of 0.601" and 0.737". The targets were in a free boundary condition, hanging from holes in the corner of each 36-inch-square flat plate. The projectiles were approximately 8 lbs and were "beveled at the nose to simulate a fan blade root impact footprint." Available test data consisted of the initial conditions plus photographs and observations of the posttest target condition. Simulation results are shown in figures 7 and 8 for tests 3 and 5. In both cases, the simulation predicted the correct amount of penetration and approximate crack patterns, which were characterized by P&W as being under-contained. The NAWC China Lake tests included the impact of an actual titanium fan blade fragment into a 0.250" thick Ti-6Al-4V panel, which was supported along two opposing edges. The target material had a lower yield strength (135 ksi) than the P&W and LLNL test materials (159 ksi). For the NAWC China Lake test simulation, the flow model was adjusted to account for the lower-strength materials and is shown in figure 9. The calculated residual velocity of 202 ft./sec compares well with the measured residual velocity of 211 ft./sec (a -4.27% error). The actual and simulated final test panel deformation are also shown in figure 9.

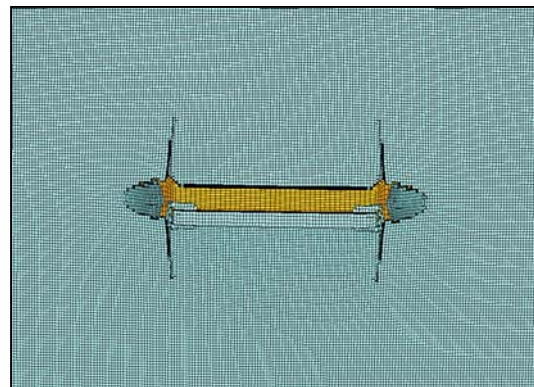
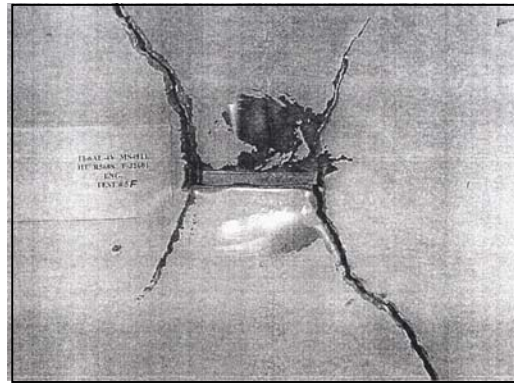
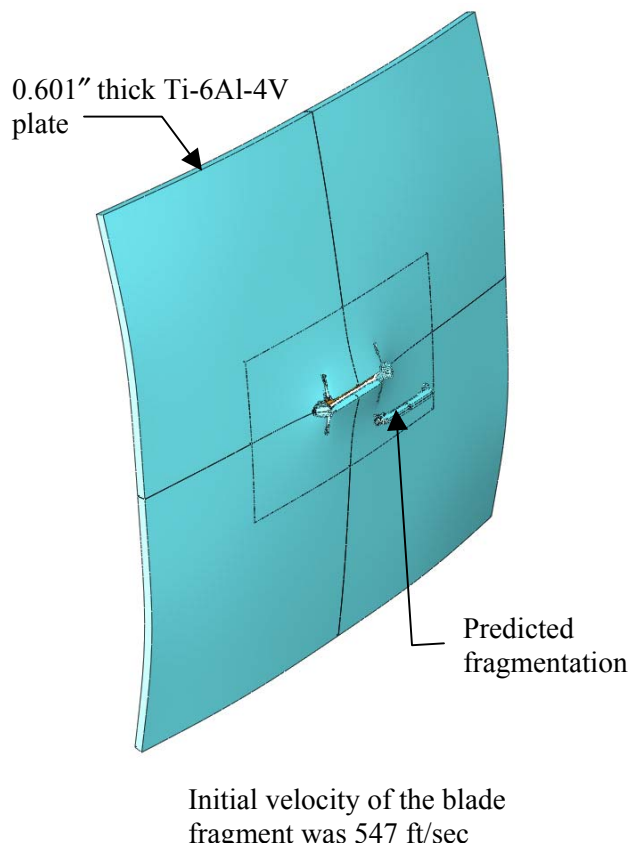
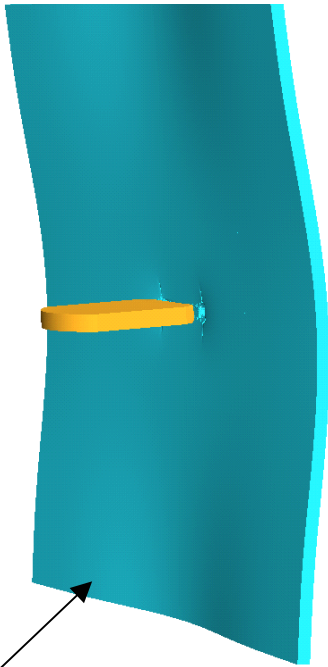


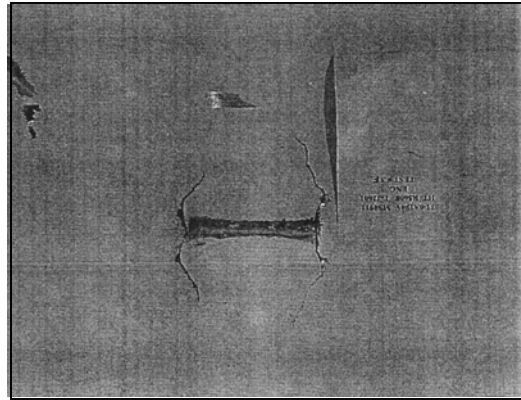
FIGURE 7. CRACK PATTERN PRODUCED BY THE JOHNSON-COOK MODEL AND THE OBSERVED PATTERN FOR P&W TITANIUM BLADE IMPACT TEST 5

Initial velocity of the blade fragment was 547 ft/sec

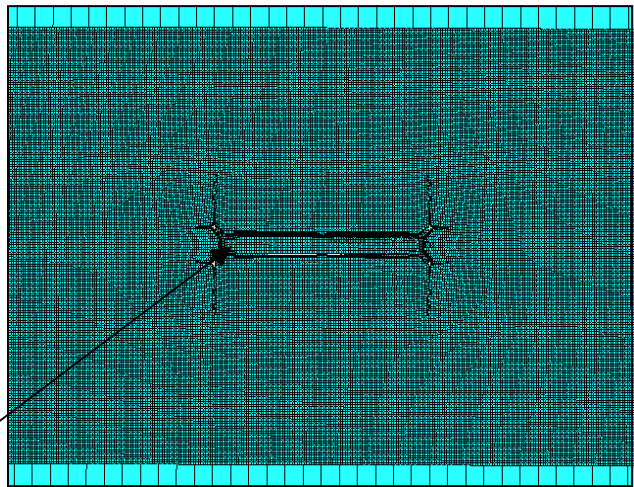


0.737" thick Ti-6Al-4V plate

Detached fragment



Rear view of P&W Shot 3



Johnson-Cook material model prediction

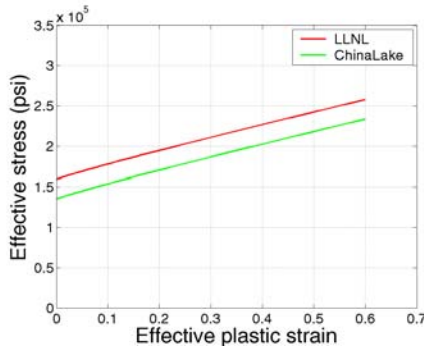
FIGURE 8. CRACK PATTERN PRODUCED BY THE JOHNSON-COOK MODEL AND THE OBSERVED PATTERN FOR P&W TITANIUM BLADE IMPACT TEST 3



Measured residual velocity = 211 ft/sec



Calculated residual velocity = 202 ft/sec, a -4.27% error. The FEA mesh contained 83,743 nodes and 70,076 solid elements.



The flow strength model was adjusted to reflect the difference between the China Lake titanium and the titanium that was tested at LLNL.

FIGURE 9. NAVAL AIR WARFARE CENTER CHINA LAKE TITANIUM PANEL IMPACT TEST 16

## 2.5 CONVERGENCE ISSUES.

Solution convergence issues were simplified in this study by maintaining close to uniform mesh resolution for the Ti-6Al-4V simulations. The through-the-thickness mesh resolutions are shown in table 1. An element aspect ratio less than 3.0 to 1.0 was maintained throughout this portion of the study. Eight-node solid brick elements with a one-point integration were employed throughout this study. The outer regions of the targets were sometimes meshed with fewer elements through the thickness (by a factor of three) and then tied to the finer-zoned impact region, to reduce the number of elements in each calculation. The finer-zoned impact region extended to between two and three times the relevant impactor dimension.

TABLE 1. SOLUTION CONVERGENCE ISSUES WERE SIMPLIFIED AFTER MAINTAINING CLOSE TO UNIFORM MESH RESOLUTION FOR THE Ti-6Al-4V SIMULATIONS

Simulation	Target Thickness (inch)	Thickness Resolution (inch/element)	Symmetry Conditions	Total Elements
Split Hopkinson bar tests	0.312	0.0167	2D-axisymmetric model	6021
P&W test 3	0.601	0.0500	3D-1/4 symmetry model	209,220
P&W test 5	0.737	0.0491	3D-1/4 symmetry model	110,400
China Lake test 16	0.250	0.0417	3D-1/4 symmetry model	70,706

### 3. 2024-T3 ALUMINUM FAILURE STRAIN PARAMETERS.

#### 3.1 2024-T3 ALUMINUM FAILURE PARAMETER DETERMINATION.

The 2024-T3 aluminum parameters for the Johnson-Cook failure strain model were determined by simulating the results of ballistic limit tests that were conducted by LLNL [5]. In those tests, a titanium fragment simulant projectile (FSP) impacted fixed boundary 0.150" and 0.100" thick, 6" by 6" 2024-T3 aluminum sheets. The FSP is a 0.050" diameter cylinder with a beveled nose. Recorded data included ballistic limit velocities and an estimation of the ballistic limit experimental variance.

The 2024-T3 ballistic limit was determined in the simulations by plotting the target fragment velocity against a range of initial projectile velocities for a complete set of failure strain parameters ( $D_1$ - $D_3$ ). These failure strain parameter sets were then varied until a satisfactory fit to the data was obtained. The results of the simulation and the experimental results are shown in figure 10 for the best fit of the Johnson-Cook failure parameters. Calculated ballistic limits deviated from the measured values by 0.6% for the 0.100" plate and 5.73% for the 0.150" thick target. The revised 2024-T3 flow surface, obtained from reference 1, that was used in the simulations is shown in figure 11. The failure parameters that were used in the ballistic limit simulation are given in figure 12. Close to uniform mesh resolutions were maintained for the 2024-T3 simulations, which are shown in table 2. An element aspect ratio less than 4.0 to 1.0 was maintained throughout this portion of the study and eight-node solid brick elements with a one-point integration were also employed. All meshes were three-dimensional in nature.

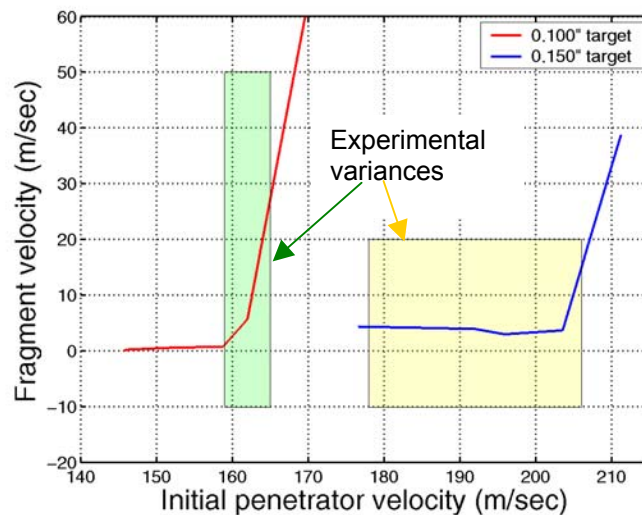


FIGURE 10. 2024-T3 BALLISTIC LIMIT SIMULATION COMPARISONS WITH LLNL EXPERIMENTAL RESULTS

Aluminum 2024-T3 yield surface parameters [1]  
 $A = 53.517$  ksi  $n = 0.73$   
 $B = 99.202$  ksi  $m = 1.7$   
 $C = 0.0083$

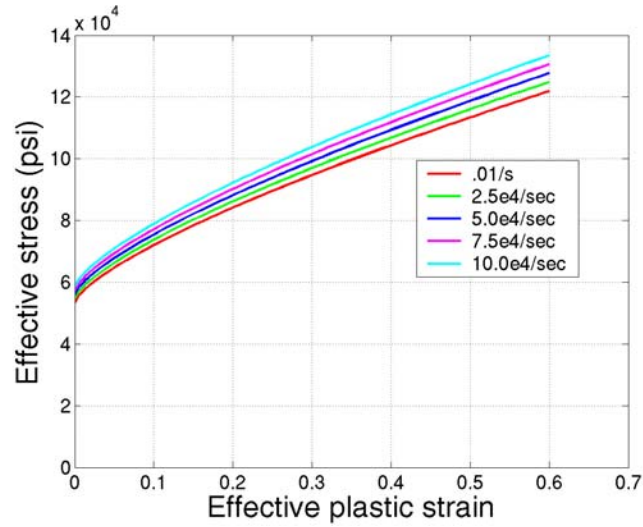


FIGURE 11. JOHNSON-COOK 2024-T3 FLOW SURFACES FOR VARYING STRAIN RATES

Aluminum 2024-T3 failure strain parameters  
 $D_1 = 0.112$        $D_4 = 0.007$   
 $D_2 = 0.123$        $D_5 = 0.0$   
 $D_3 = 1.500$

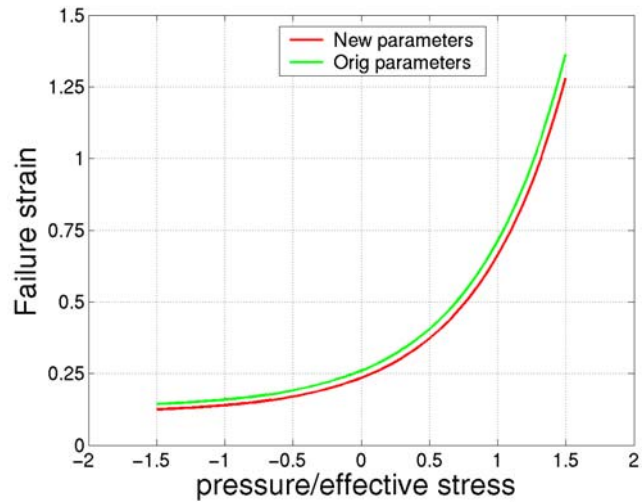


FIGURE 12. JOHNSON-COOK 2024-T3 ALUMINUM FAILURE STRAINS FOR VARYING  $\sigma^*$

TABLE 2. SOLUTION CONVERGENCE ISSUES WERE SIMPLIFIED AFTER MAINTAINING CLOSE TO UNIFORM MESH RESOLUTION FOR THE 2024-T3 ALUMINUM SIMULATIONS

Simulation	Target Depth (inch)	Target Depth Mesh Resolution (inch/element)	Symmetry Assumption	Total Number of Elements
LLNL ballistic limit	0.100	0.0125	1/4	9,936
LLNL ballistic limit	0.150	0.0125	1/4	14,304
NWAC shot 14	0.102	0.0170	none	51,940
NWAC shot 17	0.078	0.0125	none	33,388
NWAC shot 22	0.101	0.0163	none	53,276

### 3.2 2024-T3 ALUMINUM FAILURE PARAMETER EVALUATION.

The 2024-T3 aluminum failure strain parameters were evaluated on penetration tests performed by the NAWC China Lake [10]. In the NAWC China Lake tests, actual fragments from fan blades were launched into a commercial transport aircraft fuselage. Impact velocity magnitudes and orientations were recorded as well as the residual projectile velocities. The fan blade fragments weighed approximately 0.7 lb. Test targets that were simulated included fuselage skin only, fuselage skin and a hat-stringer, and fuselage skin plus an offset rib. Three of these NAWC tests were compared to LLNL simulations as follows:

- a. NAWC test 17, an impact between a blade fragment traveling 505 ft./sec and a fuselage skin panel, resulted in a residual fragment velocity of 441 ft./sec. The calculated residual velocity of 451 ft./sec is in error by 2.3%. The test and simulated final deformations are shown in figure 13.
- b. Shown in figure 14 are the results of the simulation of NAWC test 22. This was a more complicated geometry, with an aluminum hat section that was riveted to the aluminum skin approximately every 1.25" inches. The rivets were not included in the analysis and the hat section base was fully merged to the skin panel. The calculated residual velocity for test 22 was in error by -1.2%.
- c. NAWC shot 14 entailed the impact of a 0.694-pound blade fragment into a skin panel with an offset rib, which was fixed to a raised frame around the skin pane. The postshot configuration and simulation results are shown in figure 15. The simulation error of -14.1% is larger than the other two NAWC simulations and may be due to inaccuracies in the meshing of the rib section.

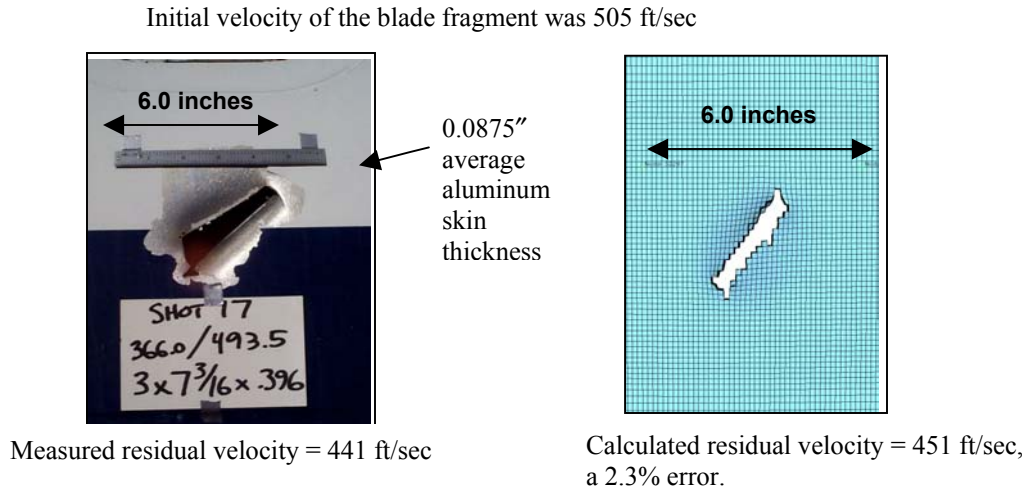


FIGURE 13. NAVAL AIR WARFARE CENTER ENGINE DEBRIS TEST 17: FAN BLADE FRAGMENT IMPACT WITH A SKIN SECTION

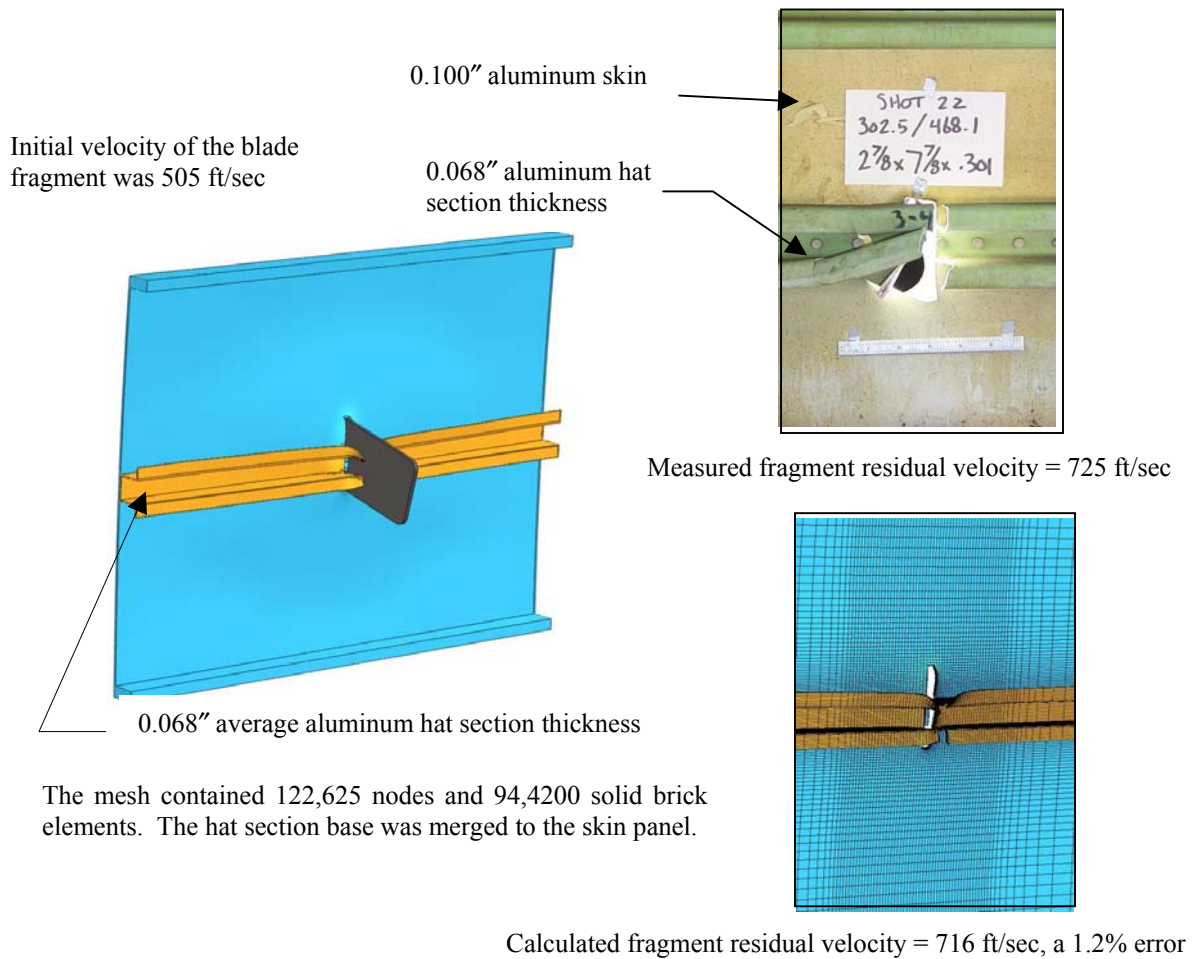


FIGURE 14. NAVAL AIR WARFARE CENTER ENGINE DEBRIS TEST 22: FAN BLADE IMPACT WITH A SKIN/HAT SECTION

Initial velocity of the blade fragment was 802 ft/sec

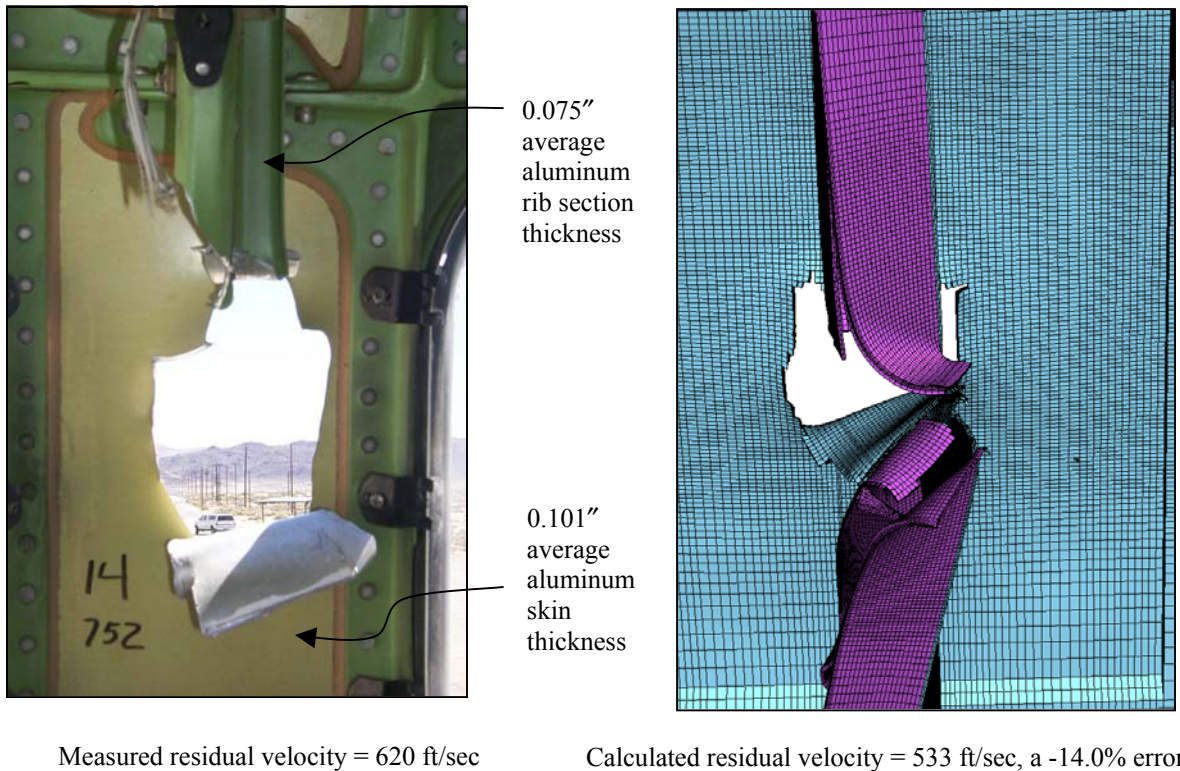


FIGURE 15. NAVAL AIR WARFARE CENTER ENGINE DEBRIS TEST 14: FAN BLADE IMPACT WITH A SKIN/RIB SECTION

#### 4. SUMMARY.

Johnson-Cook failure strain parameters were developed for Ti-6Al-4V and 2024-T3 aluminum. The titanium parameters were evaluated on two Lawrence Livermore National Laboratory (LLNL) tensile Hopkinson bar tests with 0.312" diameter specimens and differing notch radii. The titanium parameters were then successfully used to simulate Pratt & Whitney full-scale blade fragment tests on 0.602" and 0.737" thick targets and on a Naval Air Warfare Center (NAWC) China Lake full-size blade fragment test on a 0.250" thick target. The failure modes for the evaluation tests were by plugging. Failure parameters for the 2024-T3 aluminum were determined from LLNL ballistic limit tests on 0.100" and 0.150" targets. The 2024-T3 aluminum failure parameters were used to simulate three blade fragment impact tests against a commercial transport aircraft fuselage conducted by the NAWC China Lake.

Ti-6Al-4V failure parameters that were derived from scaled down ballistic limit testing produced a failure envelope that was not suitable for use on full-scale tests. Failure mode identification, material processing, and rate effects are possible causes for this inconsistency. It is recommended that they be further investigated to be able to adequately demonstrate accuracy of the material code.

## 5. REFERENCES.

1. Donald Lesuer, "Experimental Investigation of Material Models for Ti-6Al-4V and 2024-T3," FAA Report DOT/FAA/AR-00/25, September 2000.
2. Johnson, G.R. and Cook, W.H., "Fracture Characteristics of Three Metals Subjected to Various Strain, Strain Rates, Temperatures and Pressures," *Engineering Fracture Mechanics*, Vol. 21, No 1, pp. 31-48, 1985.
3. Hancock, J.W. and Mackenzie, A.C., "On the Mechanism of Ductile Failure in High-Strength Steels Subjected to Multi-Axial Stress-States," *J. Mech. Phys. Sol.*, pp. 147-175, 1976.
4. Johnson, G.R. and Holmquist, T.J., "Test Data and Computational Strength and Fracture Model Constants for 23 Materials Subjected to Large Strains, High Strain Rates, and High Temperatures," Los Alamos National Laboratory, LA-11463-MS, 1989.
5. Gogolewski, R.P. and Morgan, B.R., "Ballistics Experiments With Titanium and Aluminum Targets," FAA Report DOT/FAA/AR-01/21, April 2001.
6. Alexander, D.G. and Dietz, L.M., Pratt & Whitney memo FR-24864-8, October 12, 1999.
7. Steven J. Lundin, "Advanced Aircraft Materials Penetration Testing," Naval Air Warfare Center, China Lake, Draft Report v6, 2002.
8. Backman, M.E. and Goldsmith, W., *Int. J. Eng. Sci.*, Vol 16, p. 1, 1978.
9. Gogolewski, R.P. and Cunningham, B.J., "Terminal Ballistic Experiments for the Development of Turbine Engine Blade Containment Technology," Lawrence Livermore National Laboratory, UCRL-ID-120930, 1995.
10. Steven J. Lundin, "Engine Debris Fuselage Penetration Testing, Phase I," FAA Report DOT/FAA/AR-01/27, August 2001.